Compton Scattering

Chandrahas Gabbita

May 2023

1 Abstract

In this paper, we investigate the properties of Compton scattering and present the results of the Compton scattering experiment performed as a part of senior lab. In this experiment, gamma rays from a strong Cs-137 source were irradiated on to a cylindrical Aluminum scatterer and the radiation energy spectrum was recorded over a range of energies and angles. The data was then analyzed to produce two plots: Peak energy vs angle and the differential cross section- $\frac{d\sigma}{d\theta}$ - as a function of angle. The mass of the electron was estimated to be 511.57663302 ± 77.46keV from the Energy - Angle relationship expected for Compton scattering after fitting the appropriate function. As for the differential cross section, two different models were discussed - the classical Thompson model and the quantum corrected Klein-Nishina model - and compared with experimental data from the lab. One fit was performed for each model and the Klein-Nishina model demonstrated better agreement with the observed data as expected.

2 Introduction

Compton scattering is one of the four competing methods of photon-matter interaction and predominantly occurs at photon energies ranging between a few MeV to a few GeV. At energies below this range, photons primarily interact with matter through the photoelectric effect and ionize atoms in the sample, and at energies beyond this range, photons interact directly with the nucleus to cause pair-production. In Compton scattering, however, photons interact with the electrons in a sample and transfer some of their energy to the electrons and lose energy in the process. This phenomenon of an electron gaining energy is known as electron recoil and the photon's wavelength after the scattering is larger than it was before because of its lower energy. The energy transferred to the electron depends on the angle of scattering and the initial energy of the photon. In deriving the equation for the energy lost by a photon through this form of scattering, we assume that the electrons are at rest and that the photon has a high enough energy so that that the electrons kinetic energy is negligible. We further assume that the electron is also free and is not bound by the nucleus because the photon energy is significantly higher than the ionization energy of the atoms in the sample. Under these assumptions, we use the conservation of momentum and energy of the photon-electron system to arrive at an equation to determine the energy lost by a photon during the collision.

$$E'_\gamma = \frac{E_\gamma}{1 + \frac{E_\gamma}{m_e c^2}(1 - \cos(\theta))}$$

Where E_γ and E'_γ are the energies of the photon before and after the collision respectively, m_e is the mass of the electron, and θ is the deflected angle of the photon. This equation relates the photon energy to the angle of scattering. So in case of a photon source at a known energy such as the Cs-137 source used in this experiment, radiating photons at an energy of $661.6keV$, the value of the energy peak at any scattering angle can be determined. However, the equation doesn't discuss the probability of a photon scattering at a particular angle. In order to determine, the height of the peak - or the probability of scattering - at an angle θ, we rely on two models of differential scattering. Namely, the classical Thompson model, and the quantum mechanical Klein-Nishina model.

The Thompson model was proposed by J.J Thompson in 1904 and is based on the classical theory of electromagnetism. Thompson treated the electron as a classical point particle and the incident photons classically as a plane wave. The wave would interact with the electron and be scattered at an angle. However, this model is unable to account for the change in the photons wavelength as that arises from the quantum nature of photons. However, this model is a decent approximation at low energies and angles. The scattering cross section Thompson proposed was the following:

$$\frac{d\sigma}{d\Omega} = \frac{r_0^2}{2}(1+\cos^2\theta)$$

Where r_0 is the classical electron radius ($2.81fm$).

The Klein-Nishina model was first derived in 1928 by Oscar Klein and Yoshio Nishina and correctly treats the photon as a particle and accurately predicts the increase in wavelength of the scattered photon. The Klein-Nishina equation is given by:

$$\frac{d\sigma}{d\Omega} = \frac{r_0^2}{2}\frac{(1+\cos^2\theta)}{[1+\gamma(1-\cos^2\theta)]^2}[1+\frac{\gamma^2(1-\cos^2\theta)^2}{(1+\cos^2\theta)(1+\gamma(1-\cos\theta))}]$$

Where, again, r_0 is the classical electron radius and γ is the ratio of the photon energy to the electron rest energy - $\gamma = \frac{E_\gamma}{m_e c^2}$.

The Klein-Nishina formula can be deceiving since at first glance it appears to be missing the planks constant, h, even though it is a quantum mechanical equation. However, this is not the case since the planks constant is present in γ.

Experimentally, the differential scattering cross-section can be determined through the following relationship:

$$Y(\theta) = N_e N_\gamma \epsilon \frac{d\sigma}{d\Omega} d\Omega$$

Where, $Y(\theta)$ is the number of scattered photons at angle θ, N_e is the number of electrons in the scatterer that interact with the photon beam, N_γ is the number of photons that bombard the scatterer, ϵ is the efficiency of the detector, $d\Omega$ is the solid angle of the detector, and finally $\frac{d\sigma}{d\Omega}$ is the scattering cross-section.

This relationship is used to determine the scattering cross section experimentally and verify the accepted theoretical models of scattering.

3 Experimental Setup

The setup of the experiment consisted of a Cs-137 γ-source that emitted photons at a known energy, a scatterer, and a rotatable detector to record the energy spectrum at various angles. Cs-137 was chosen for the source in this experiment since we know its decay peak is located exactly at $661.7keV$. The Cs sample was completely enclosed in a lead "house" except at the front of the house where the γ-beam from the sample could exit the encasing and scatter on to a scatterer placed directly in front of the source. The main scatterer in this experiment was a large Al cylinder but for the last part of the experiment, two small Cu and Al cylinders were used instead. The detector was permanently fixed on to a rotatable piece of wood that could be freely rotated about the scatterer such that the detector was at a fixed distance to the scatterer at all times. The detector is a $3in \times 3in$ cylindrical NaI crystal doped with Tl to give $NaI(Tl)$. Doping changes the valance structure such that the crystal emits photons when incident photons strike it. The detector is connected to a photo-multiplier tube (PMT) which amplifies the signal sufficiently to be detectable. The output of the PMT is connected to the pre-amplifier, amplifier, and multi-channel analyzer (MCA). The multi-channel analyzer digitizes the signal and displays the frequency of detected events as a function of the energy of the photon.The figure below depicts the experimental setup used.

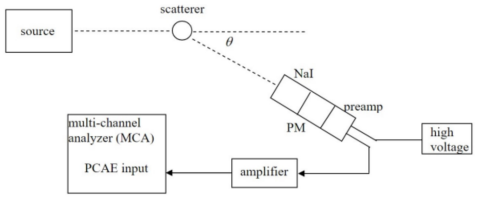

Figure 1: Schematic of Experimental Setup

4 Results and Analysis

4.1 Calibration

The MCA provides frequency data of the observed decay events at each energy in the range of the detector. In order to do so, the photon (or event) is binned into one of the many energy bins that comprise of the full spectrum range in the software based on its energy. However, the MCA does not provide the energy of a particular bin in the software. Therefore, it is vital we calibrate the experiment to determine the relationship between the bin number in the software and the observed photon energy before analyzing data. This calibration was performed by choosing specific radioactive samples such as ^{137}Cs, ^{22}Na, ^{133}Ba, and ^{57}Co with known energy peaks. These samples were placed immediately next to the detector and the spectrum was collected. Since we know the value of the energy peaks, and the bin number associated to that energy from the software, we can find a relationship between them. The relationship between bin number and energy was assumed to be linear and after multiple data points from different samples were collected, the data was plotted in an Energy vs Bins plot. A line

was fitted through the data and the conversion between bins and energy was determined. The plot of the calibration data and the regression line is shown in the figure below.

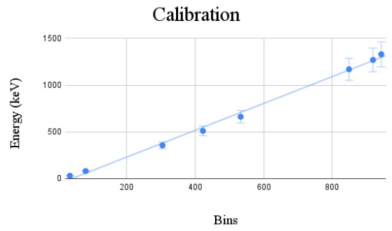

Figure 2: Calibration data - Energy vs Bins plot

The fit obtained from the plot was [Energy(keV)] = 1.38[Bin number] − 58.7keV

4.2 Compton Energy-Angle Relationship

As discussed in the introduction, the scattered photon energy is expected to drop with an increase in scattering angle. The relationship is expected to follow the equation below.

$$E'_\gamma = \frac{E_\gamma}{1 + \frac{E_\gamma}{m_e c^2}(1 - \cos(\theta))}$$

We test this relationship by collecting photon energy data at different angles corresponding to different scattering angles of the detector and fitting the relationship to observed data. In order to obtain accurate peak data without background noise, for each angle, two data sets were collected - one with the incident beam, and one with just the background without a beam. The background noise was subtracted from the scattering data taken with the beam. This was done for the following angles: $18^o, 20^o, 25^o, 30^o, 40^o, 50^o, 65^o, 80^o, 95^o, 110^o$. For this section, the scatterer used was the main large *Al* scatterer discussed in the previous sections. Data from the MCA was collected and the frequency-bin data was converted to frequency-energy using the calibration obtained above. This gave us a set of 10 full energy spectrum datasets corresponding to each of the 10 detector angles. The data had the form (*Counts vs Bins*), where counts is the number or frequency of photons detected in a specific energy bin. Since the energy peak location of the source is known, 661.7keV, we expect the peak location to recede further to the left on the frequency-bin plot corresponding to a decrease in scattered photon energy. In order to determine the location of the peak, a curve was fit to each of the datasets assuming the peaks were gaussian and the background noise remaining after subtraction had a polynomial form. For the regression model, the uncertainty and distribution in the counts or frequency data was determined as follows. Since the probability of the detector detecting a photon in a certain energy bin follows the possion distribution, with the mean λ being best estimated by the value of frequency of photons detected in that energy bins (*Counts*), the variance of the distribution was assumed to be $\sigma^2 = Counts$. Giving us a standard deviation of $\sqrt{Counts}$. Therefore, for each energy bin, the data had the form

$$Counts \sim Counts \pm \sqrt{Counts} \text{ , Poisson}$$

. Further simplification can be made after noting that the counts are sufficiently large for the poisson distribution to approximate the normal distribution with $\mu = Counts$ and $\sigma^2 = Counts$. Therefore, standard regression techniques such as the weighted-least squares could be used without modification and the form of our data becomes:

$$Data \sim N(Counts\ ,\ Counts)$$

However, the data obtained was noted to have skewed and asymmetric peaks opposing the assumption that the peaks were gaussian. This was due to the efficiency of the detector depending on the energy of the scattered photons. As can be seen from the appendix, the probability of detecting a photon at a certain energy exponentially decreases with energy. Therefore, the corrected number of counts depends on the measured counts as follows.

$$Counts_{measured} = \epsilon \times Counts_{corrected}$$

Where ϵ is the efficiency of the detector. The efficiency was determined from the log-log plot in the appendix.

Finally, it was observed that the data contained two peaks and an approximately zero background. However, for the sake of flexibility, the regression model was assumed to be a sum of two gaussians and a quadratic background.

$$D \sim N(\mu_1, \sigma_1^2, h_1) + N(\mu_2, \sigma_2^2, h_2) + aE^2 + bE + c$$

Where μ is the mean, σ is the standard deviation, and h is the height of each gaussian, E is the energy of the photon (x- axis), and a, b, c are regression parameters that determine the background polynomial. After correcting for efficiency, and accounting for uncertainties, a weighted-least-squares fit was performed for eacch of the 10 angles. An example of the fit performed is in the figure below.

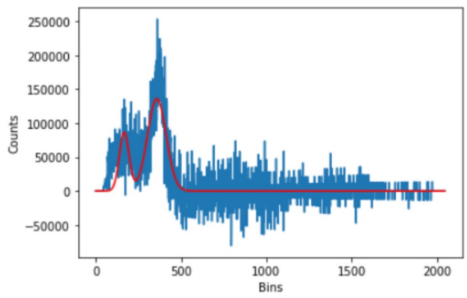

Figure 3: An example of the fit discussed

Upon fitting the 10 datasets, the location of the 661.7 keV peak was traced by extracting the μ_2 parameter from the fit. The uncertainty in μ_2 was taken to be the standard deviation of the peak σ_2. These results were plotted in the Counts vs Bins plot shown below.

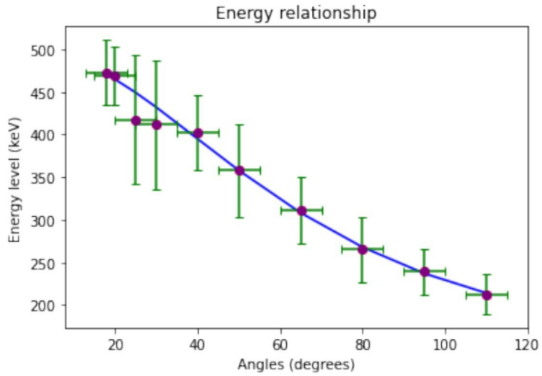

Figure 4: Energy Angle relationship with fit

The expected energy angle equation for Compton scattering was used to fit the observed data. In fitting the function, it was assumed that the mass of the electron (m_e) was unknown and weighted-least-squares was used to determine m_e. m_e was obtained to be 511.576 ± 77.6 keV, with a χ^2 value of 0.039.

4.3 Differential Scattering Cross-Section

As mentioned in the introduction, the differential cross section is given by:

$$Y(\theta) = N_e N_\gamma \epsilon \frac{d\sigma}{d\Omega} d\Omega$$

We have determined the total efficiency in section 4.2 and corrected our data. Therefore, we have already computed $\frac{Y(\theta)}{\epsilon d\Omega}$. Therefore, we can rewrite the equation with corrected data as:

$$Y'(\theta) = N_e N_\gamma \frac{d\sigma}{d\Omega}$$

In addition, we know the geometry of the scatterer so we calculate the number of electrons present in it using its density. We found that a good approximation was to take the area of the scatterer equal to that of the detector. Similarly, we compute the number of photons radiated by the ^{137}Cs source using the fact that the sample was purchased in 1978 when its activity was $300\mu Cu$. We simply calculate the radioactivity in 2023 based on its half-life. Therefore, we need only compute the number of counts present in the peaks, $Y'(\theta)$. In order to compute $Y'(\theta)$, we sum up the number of counts within the interval $\mu_2 \pm \sigma_2$. This accounts for the uncertainty in the peak due to the imperfect detection from the detector. Theoretically, the 661.7keV peak should be a dirac delta peak. However, because it is impossible for the detector to detect such a peak without a spread, we account for this by summing up counts within one standard deviation of the peak maximum. Since the counts at each energy bin (i^{th} bin) has the form

$$D_i \sim N(Counts_i, Counts_i)$$

The sum of counts within one standard deviation is expected to have the following distribution

$$\Sigma D_i \sim N(\Sigma_i Counts, \Sigma_i Counts)$$

The differential cross section was then calculated and the plot is shown below

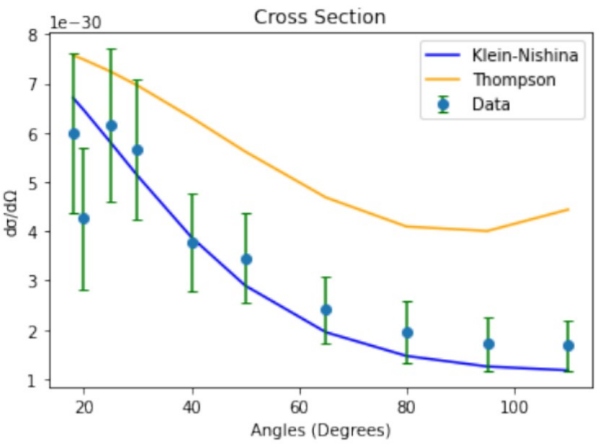

Figure 5: Scattering cross section with the expected curves based on the Thompson and Klein-Nishina models

Both expected curves from the Klein-Nishina and Thomson models of differential scattering were plotted along with the observed data. It is clear that the Klein-Nishina is in better agreement with the observed data. The Thompson model had a χ^2 of 89.2 and the Klein-Nishina model had a χ^2 of 5.825.

4.4 Comparison of cross section measurements of Al and Cu

In this section, the cross sections of Al and Cu are compared for angles 25^o and 45^o. In order to do so, we determine the ratio of the count for both materials at the mentioned angles. In this section, the large Al scatterer has been removed and the small Al and Cu scatterers have been used. The data for the counts was highly noisy. As a result a moving average was performed to eliminate some of the noise. The chosen window size was 75. The distribution of the data after the moving average was performed is expected to be

$$\frac{\Sigma_{window}\, Counts_i}{\text{windowlength}} \sim N(\frac{\Sigma Counts_i}{\text{windowlength}}, \frac{\Sigma Counts_i}{\text{windowlength}})$$

This cleaned data was then fit with a gaussian and a polynomial background similar to the model used in section 4.2. The polynomial fit was then subtracted from the data since the data wa still highly asymmetric and couldn't be accurate fit with gaussians. Finally, using the same procedure outlined in section 4.2, we added the counts within one standard deviation of the location of the peak to obtain the corrected counts data that can be used to calculate the ratio. The ratios obtained for 25^o and 45^o were 0.7118 ± 0.4399 and 0.8032 ± 0.3610 respectively. The ratios are close to 1 within uncertainty.

Therefore, it is trivial to calculate the number of free electrons in Al and in Cu. In Al we get $(8.013 \pm 2.17) \times 10^{29}$ and in Cu, we get $(3.196 \pm 1.091) \times 10^{29}$.

5 Conclusion

In conclusion, in this paper, we have verified the theory of Compton scattering including the expected Energy-Angle relation, checked the accuracy of two conventionally used models of Compton differential scattering - Thompson and Klein-Nishina models - and calculated the number of free electrons in Cu and Al.

We began by collecting the full energy spectrum of the scattered γ beam at angles $18^o, 20^o, 25^o, 30^o, 40^o, 50^o, 65^o, 80^o, 95^o, 110^o$ giving us 10 datasets. We then calibrated the MCA to determine the relationship between the Energy and Bin number using 4 different elements with known energy peaks. Upon determining the calibration, the 661.7keV peak was traced across angles to determine the relationship between Angle and Energy. The theoretically accepted relationship given by

$$E'_\gamma = \frac{E_\gamma}{1 + \frac{E_\gamma}{m_e c^2}(1 - \cos(\theta))}$$

was used to determine the mass of the electron. The electron mass was determined to be 511.576 ± 77.46 keV with the χ^2 for the fit being 0.039. This agrees very well with the accepted literature value of electron mass. Next, the differential scattering cross section was determined using the relation

$$Y(\theta) = N_e N_\gamma \epsilon \frac{d\sigma}{d\Omega} d\Omega$$

Two conventionally accepted equations for the cross section were then fit - namely, the Thompson model and the Klein-Nishina model. It was shown that the quantum corrected Klein-Nishina model agreed better with the observed data with a χ^2 value of 5.825. The χ^2 value for the Thompson model was 89.2. Finally, the ratio of scattering cross sections was determined for two small Al and Cu scatterers an the number of free electrons in each scatterer were determined. The number of free electrons calculated in Al were $(8.013 \pm 2.17) \times 10^{29}$, and the number of free electrons calculated in Cu were $(3.196 \pm 1.091) \times 10^{29}$.

6 Appendix

In the appendix, we present further plots and data that were used in the data analysis above but haven't been presented in their respective sections.

1. Plot of total efficiency of the detector (log -log plot)

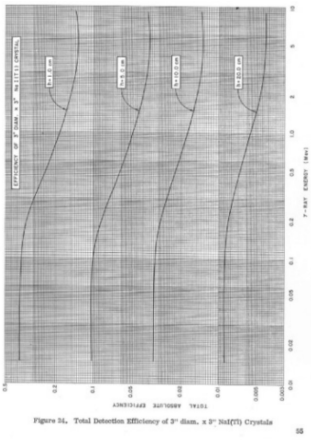

Figure 6: Plot of total efficiency of a $3in \times 3in$ NaI detector

2. Plot of efficiency ϵ as a function of bin number (linear plot)

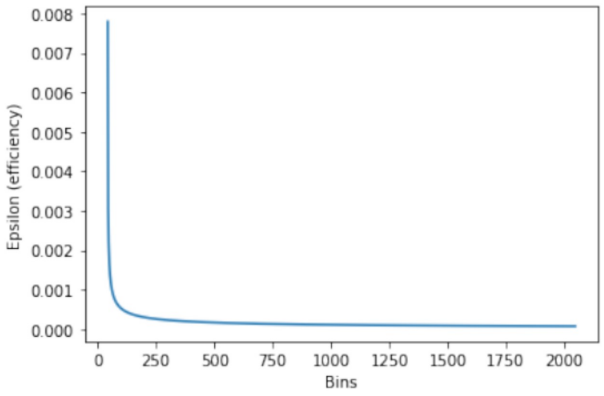

Figure 7: Total efficiency ϵ in linear scale as a function of bin number

7 References

1. Compton Scattering Lab Report Write Up, Stony Brook University, PHY 445